Crater evolution after the impact of a drop onto a semi-infinite liquid target

Alfio Bisighini and Gianpietro E. Cossali
Facoltà di Ingegneria, Università di Bergamo, via Marconi 6, 24044 Dalmine (BG), Italy

Cameron Tropea and Ilia V. Roisman
Institute of Fluid Mechanics and Aerodynamics, Center of Smart Interfaces, Technische Universität Darmstadt, Petersenstraße 30, 64287 Darmstadt, Germany

(Received 3 February 2010; revised manuscript received 27 July 2010; published 24 September 2010)

This paper is devoted to an experimental and theoretical investigation of the crater formed by the impact of a single drop onto a semi-infinite target of the same liquid. The shape of the crater at various time instances after impact has been observed using a high-speed video system and then accurately characterized. A theoretical model for the crater expansion has been developed, which is able to predict the temporal variation of the crater depth for sufficiently high Weber, Froude, and Reynolds numbers. The flow around the crater is approximated by an irrotational velocity field past a moving and expanding sphere. The equations describing the propagation of the surface of the crater have been obtained from the balance of stresses at the crater interface, accounting for inertia, gravity, and surface tension. The temporal evolution of the crater depth has been calculated by numerical solution of the equations of motion. The agreement between the theoretical predictions and experimental data are rather good.

DOI: 10.1103/PhysRevE.82.036319 PACS number(s): 47.55.dr

I. INTRODUCTION

Worthington [1] is the pioneer in the field of experimental observations of drop impact, who spent on this study about 20 years at the turn of the 19th century. He used powerful sparks from Leyden jars to create the necessary brief exposure time for the first high-speed drop images. High-resolution, high-speed video systems which have appeared over the last years now allow us to easily observe the smallest details of such flows [2].

Crater formation by drop impact has been studied, as reviewed by Prosperetti and Oğuz [3], because of its relation to underwater noise of rain, which in turn permits the detection and characterization of rain over the oceans by remote acoustic sensors. Phenomena of drop impacts on liquid layers are also related to various engineering applications in which secondary spray atomization by collision with a wall, spray deposition and coating, and spray cooling play an important role. The wall flow generated by spray impact is rather complicated and is still not completely understood [4–6]. In order to model and predict the outcome of spray/wall interaction an accurate prediction of the typical sizes of the crater formed by single drop impact and the characteristic time of its formation and collapse is necessary. Moreover, a simplified description of the liquid flow generated by drop impact is required in order to reliably model the heat transfer associated with spray cooling [7].

A. Existing experimental data for the penetration depth: do we need more?

The Weber, Froude, and Reynolds numbers are usually applied to describe the phenomena of drop impact: $\mathrm{We}=\rho V^2 D/\sigma$, $\mathrm{Fr}=V^2/(gD)$, and $\mathrm{Re}=\rho VD/\mu$, where ρ, μ, σ are the density, the viscosity and the surface tension of the target liquid, D and V are the diameter and velocity of the impacting drop. However, a consensus exists that in most cases the effect of viscosity is negligibly small and the problem is completely described using We and Fr.

In order to examine the existing data about maximum depth of crater penetration we collected numerous existing experimental data sets from several relatively narrow ranges of Froude number. We could expect that the corresponding values for the maximum penetration depth will be constant (for very high Weber numbers) or will monotonically increase with We, since the Reynolds number is high in all the cases. The results are shown in Fig. 1. Each symbol in Fig. 1 corresponds to a different source among [8–14]. The scatter of the data from these different sources is rather significant, which could indicate that either the expected monotonic increase of $\Delta_{\max}$ with We is not valid or that some of the existing experimental data are not reliable. An analogous correlation is shown in Fig. 2. In this figure the data from relatively narrow ranges of the Weber number are shown as function of the Froude number.

Experimental results can be potentially influenced by the refraction of the light beams in the water, the measured values of length depend on the camera orientation and distance from the cavity and from the wall of the container, liquid meniscus can obscure the exact position of the impact point, etc. The uncertainty of the existing experimental data on the geometry of the crater has been questioned before [12,15].

The difficulty remains that we currently cannot precisely know which data from the many existing sources are reliable, and which can be used for model validation. In the present study the potential sources of experimental error have been quantified with care with care and the results are therefore considered rather reliable.

B. Do we need a new model?

When a single drop impacts onto a deep pool with high velocity it creates an expanding, nearly spherical cavity. The

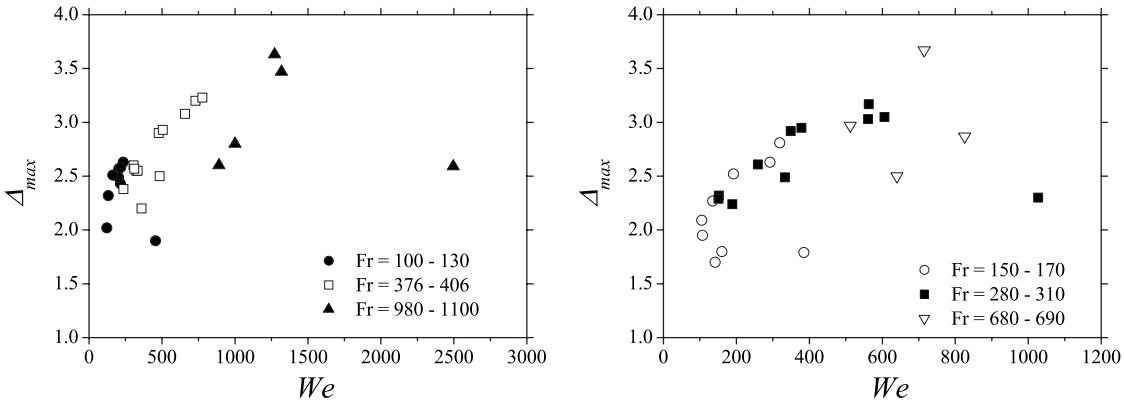

FIG. 1. Existing [8–14] experimental data for the dimensionless maximum crater depth Δ_{max} (scaled by the initial drop diameter) from several narrow ranges of the Froude number plotted as function of the Weber number.

cavity first penetrates into the liquid pool and then recedes under the action of surface tension and gravity. Most of the existing models of drop impact presented in the literature deal with predictions of the maximum crater depth. All the models, which are usually based on the consideration of the energy balance, are formulated with the assumption of a hemispherical shape for the crater, centered on the impact point [3,11–14,16,17]. Engel [18] found an analytic expression for the crater evolution in time, using the energy balance equation and assuming a kinematically admissible irrotational flow around the expanding crater. The assumption of irrotational flow around the crater was confirmed later by [19], who pointed out that when the drop hits the pool surface, very little vorticity is generated by the impact. During the subsequent development of the crater, vorticity production at the free surface is minimal in view of the fact that Reynolds number is of order of thousands.

The simple flow generated by the point source is in fact widely used in impact cratering studies [12,20,21]. Such a flow has been used in [22] for the description of the pressure field around the crater. The equations of the crater expansion are obtained from the kinematic and dynamic boundary conditions at the free surface of the spherical crater. An analytical expression for the crater radius and depth is then obtained, which agrees well with the experimental data for the relatively early stages of crater penetration. This model does not predict crater maximum penetration depth and receding since the surface tension and the gravity are not taken into account.

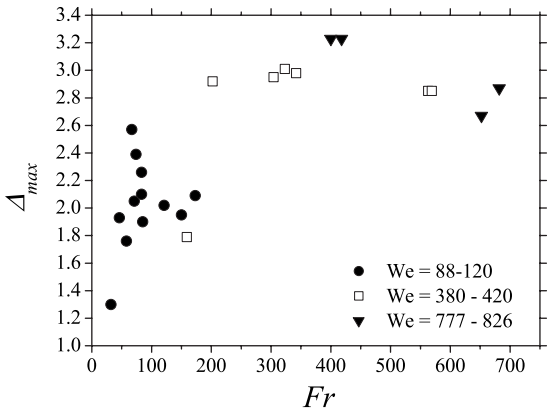

FIG. 2. Existing [8–14] experimental data for the dimensionless maximum crater depth Δ_{max} (scaled by the initial drop diameter) from several thin ranges of the Weber number plotted as function of the Froude number.

There are two main disadvantages of almost all existing theoretical models for cavity expansion. The first problem relates to the use of an *energy balance*. It is well-known that such an approach is among the lowest level theoretical tools and can provide only appropriate scales of the problem. It has been demonstrated in [23] that the energy balance cannot correctly describe even the simplest flows, for example the flow generated by formation of a rim at the edge of a free sheet (compare the results of Dupré [24] obtained using the energy balance and the correct predictions of Taylor [25] for the rim velocity) or axisymmetric spreading of a liquid disk. In the case of drop collision with a deep pool, an energy balance cannot easily capture the energy lost due to generation of the spreading waves or the energy spent on splash and secondary atomization.

The second disadvantage is in the approximation of the cavity shape by an *expanding sphere with a center fixed at the impact point*. Our experiments show that such an approximation is not precise. It is well known that in many cases gravity effects significantly influence the cavity propagation. The flow generated by an expanding sphere is symmetric, it leads to a uniform distribution of the stresses on the surface of the cavity and thus it is not able to correctly describe the pressure gradient associated with gravity.

On the other hand, simplified hydrodynamic models have been successfully applied in penetration mechanics [26–30] for description of analogous problems of relatively high-velocity penetration and deformation of jets, rods, and projectiles into metal targets.

C. Subject of this study

The main aim of the present study is to develop a model which describes the flow generated by a cavity and predicts the temporal evolution of its geometry. In the experimental part of this study the evolution of the crater is observed using high-speed video and analyzed by image processing. Many efforts have been made in order to avoid large measurements

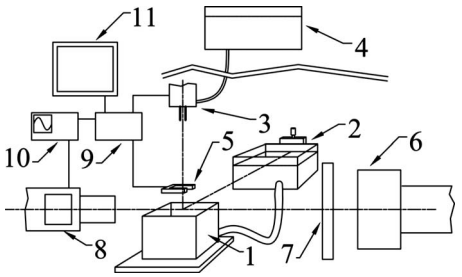

FIG. 3. Scheme of the experimental setup.

errors and to obtain a reliable and reproducible data for the time evolution of the main geometrical parameters of the crater.

A theoretical model of the type considered in [27–29] is developed which is aimed at predicting the dynamics of the crater penetration. It is based on the assumption of an irrotational velocity field around the crater, associated with a moving and expanding sphere in an inviscid liquid. The pressure field in the target liquid is then obtained from the nonstationary Bernoulli equation, which accounts for the liquid velocity and acceleration, and gravity. The equations of motion of the crater are obtained from a balance of stresses at the crater surface, accounting for surface tension and viscosity. The resulting system of ordinary differential equations is then solved numerically, using initial conditions obtained from experimental data and theoretical predictions. The model is validated by comparison with the experimental data for a wide range of impact parameters. The agreement is rather good.

The resulting velocity field generated by crater penetration can then be applied to the description of the convective heat transfer in the case of nonisothermal drop impact, an important step for the modeling of spray cooling.

II. EXPERIMENTAL INVESTIGATION

A. Experimental method

The impact of drops on a pool of the same liquid has been observed using a high-speed video system. Distilled water and acetic acid were used as working liquids for both drops and pools.

A sketch of the experimental setup is shown in Fig. 3. The target pool (1) is placed on a level platform and it is connected to a level pool (2) mounted on a vertical micrometric stage. Drops generated with a dripper (3), fed by a reservoir (4), are detected by a light sensor (5). The light emitted by a lamp (6) is diffused by a etched glass (7). The components are controlled and synchronized with electronic cards 9, a wave generator 10 and a graphical user interface 11. The impact velocity was varied by changing the fall height. All the experiments were performed under atmospheric conditions. The camera (8) was mounted on a tilting, rotating and movable platform which allows adjustment of the liquid surface normal to the field of view.

TABLE I. Values of density ρ, viscosity μ and surface tension σ for the fluids at the reference temperature 30 °C.

	ρ (kg/m^3)	μ (kg/ms)	σ (N/m)
Water	996	0.80×10^{-3}	71.22×10^{-3}
Acetic acid	1040	1.04×10^{-3}	26.63×10^{-3}

The target fluid has been heated due to the high intensity illumination. Its constant temperature was about 30 °C. The physical properties of the liquids at this temperature are reported in Table I.

When liquid interfacial phenomena are observed through a container, the liquid meniscus, formed at the interface between the liquid surface and the transparent wall obscures the area close to the interface. To avoid this effect the container was filled to the rim in order to use it as a pinned contact line [8,12,31]. In order to accurately regulate the level of the water in the container it was connected by a flexible tube to a liquid reservoir placed on a micrometric vertical stage.

To correct the image distortion due to the light refraction in the liquid the images have been calibrated separately in the regions corresponding to the liquid and air. Recorded images have a spatial resolution of about 14.50 px/mm in air and 14.33 px/mm in water. Further image analysis included automatic image background removal and edge detection using a Laplacian of Gaussian filter, estimation of the average drop velocity and collision instant, and evaluation of the main geometrical parameters of the crater. Analysis was run together with a graphical interface showing frame-by-frame the edges of the detected features superimposed onto the original image and allowing visual control by the user. For each impact condition several acquisitions were performed to check repeatability.

TABLE II. List of impact parameters and the results for the dimensionless maximum crater depth Δ_{max} and the corresponding time instant τ_{max}. Case *d* is shown in Fig. 4.

Case	Fluid	D (mm)	V (m/s)	We	Fr	Re	Δ_{max}	τ_{max}
a	Water	2.2	2.4	170	262	6391	2.44	14.83
b	Water	1.8	3.0	226	489	6774	2.55	17.48
c	Water	2.3	3.6	406	569	10128	2.82	20.54
d	Water	2.8	4.2	683	620	14638	2.93	22.01
e	Acetic acid	2.9	4.4	2190	694	12687	3.11	27.08

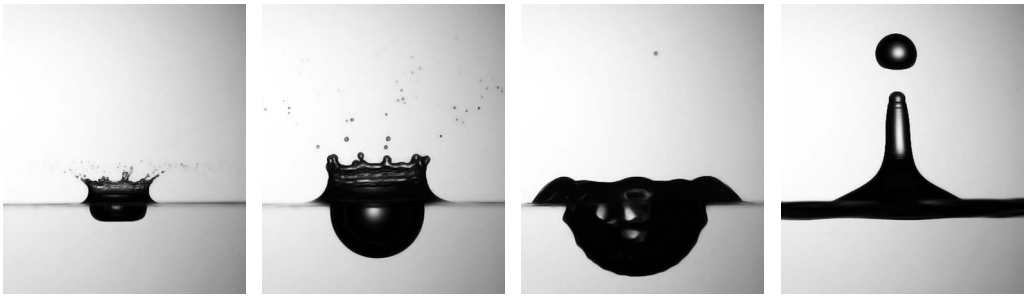

FIG. 4. Drop impact onto a semi-infinite liquid target in the splashing region (water, $D=2.8$ mm, $V=4.2$ m/s, We=683, Fr=620, Re =14 638.

Five selected cases are presented in Table II. Some variables and parameters in this study will be presented in the dimensionless form. They are scaled using D as the length scale, V as the velocity scale, and D/V as the time scale.

B. Experimental results

A typical time sequence of drop impact is shown in Fig. 4. It is interesting that in this case that the crater and the crown reach their maximum size at about the same time. Then the crown begins to fall down, generating capillary waves which travel to the bottom of the receding crater [22], after which a central jet is ejected. At higher velocities the thin liquid sheet forming the crown may rise up further and possibly neck in, forming a dome above the crater, as shown in Fig. 5. A downward jet is then formed, which falls toward the raising crater and may or may not intersect it and encapsulate one or more air bubbles in the target liquid. Successively the crater and the liquid sheet reach an equilibrium configuration with a shape similar to a toroidal bubble, which is maintained briefly until it is broken by instabilities. In this case capillary waves have not been observed on the crater.

In this study, the crater depth was measured detecting the impact point O and the lower point C on the symmetry axis (see Fig. 6). Crater width was measured detecting the top left and right points A and B, a little below the water level to avoid capillary waves from perturbing the horizontal projection. Figure 7 show the evolution in time of the dimensionless crater depth Δ scaled by the initial drop diameter D. The curves corresponding to the relatively high Weber numbers, see cases $c-e$, are rather smooth which indicates that the amplitude of the capillary waves on the crater surface is minor. At smaller Weber numbers, corresponding to the cases a and b, the effect of surface tension is significant and the evolution of the crater depth is influenced by the propagation of the waves. The corresponding graphs for the crater width Ω are shown in Fig. 8. It is interesting that even after the penetration depth reaches the maximum the crater depth continues the tendency to grow. Also the effect of the capillary waves on the cavity interface is more pronounced on this graph.

Due to a different behavior of depth and width evolution, the shape factor $\epsilon=\Delta/\Omega$ of the crater is not constant, but varies in time, as shown in Fig. 9. It is also obvious that the crater is not a perfect hemisphere with its center at the impact point (which would correspond to $\epsilon=1/2$), as considered in all of the previous analytical models.

III. THEORETICAL MODEL FOR CRATER EVOLUTION

In order to develop a simplified model for crater formation we subdivided it into two main phases, illustrated in Fig. 10. During the first phase, $\tau<\tau^*$ (τ being the dimensionless time), the drop deforms, generating a thin, radially expanding liquid layer. The material interface between the drop liquid and the target liquid is not visible during this stage. The motion of this interface is governed by the balance of the

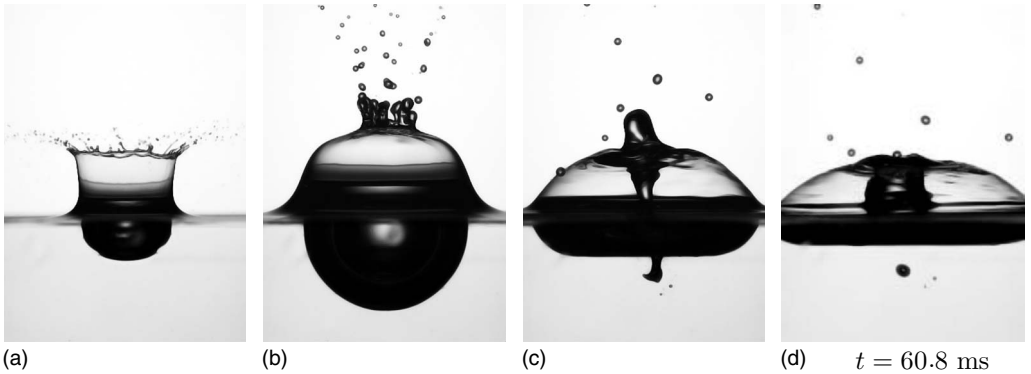

FIG. 5. Drop impact onto a semi-infinite liquid pool with formation of a toroidal bubble above the target surface and the entrapment of a bubble in the pool (acetic acid, $D=2.9$ mm, $V=4.4$ m/s, We=2177, Fr=691, Re=12 642, Bo=1.25).

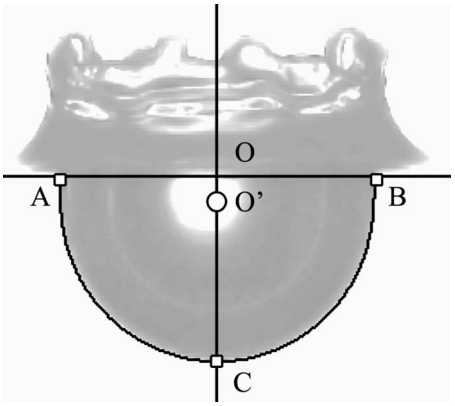

FIG. 6. Detection of the crater and of its characteristics points. O is the impact point, A, B, and C are the top left, right and bottom points, which may be fitted by a circle having center in O'.

stresses generated by the flow of the drop and pool liquids. The velocity of penetration of the drop/target interface at the time period $\tau < \tau^*$, is approximately half of the impact velocity. This result is well known from penetration mechanics [26,30] and was previously used for the description of drop impact [11,22]. The approximate dimensionless rate of drop erosion is therefore approximately 1/2. The typical dimensionless time of drop deformation is thus $\tau^* \approx 2$.

At times $\tau > \tau^*$ on the crater surface a thin residual liquid layer of the drop material is formed. During this phase the cavity shape can be well approximated by the shape of the drop/target interface. The inertial effects associated with the flow in this layer are negligibly small and the dynamics of cavity expansion can be analyzed considering conventional boundary conditions of a free surface. Crater expansion is governed by the inertia of the flow in the liquid pool and decelerated by capillary forces and gravity.

At some time instant the cavity reaches a maximum penetration depth and starts to recede. The receding phase is influenced significantly by the capillary waves generated by the falling crown [22]. Moreover, the interaction of these waves leads to the creation of the central jet. These phenomena affect significantly the dynamics of cavity collapsing. Their analysis is out of scope of the present study.

A. Flow field in the liquid pool

In the absence of gravity a spherically symmetric flow and stress fields can be found which satisfy the boundary conditions at the crater surface [22]. The pressure gradients associated with gravity destroy the spherical symmetry of the pressure field. Therefore, gravity effects cannot be precisely accounted for using the simple flow associated with the expansion of a spherical cavity with fixed center. In this study the cavity expansion is approximated by combination of the sphere expansion and its translation along the impact axis.

Consider a reference frame fixed at the impact point O with the x axis lying on the unperturbed liquid surface and the z axis (impact axis) directed normal to it, as in Fig. 11. Consider also a moving spherical coordinate system $\{r, \theta, \varphi\}$ with the origin at the center O′ of the spherical cavity, where r is the radial coordinate and θ is the zenith angle. The radius of the crater in the relative spherical reference system is denoted by $a(t)$ and the position of its center on the symmetry axis by $z_c(t)$.

The potential ϕ of a relative irrotational flow around the cavity in the moving coordinate system satisfying the Laplace equation $\Delta\phi = 0$ can be easily obtained as a superposition of a flow past a sphere and the radially expanding flow generated by sphere expansion,

$$\phi = -\dot{z}_c r\left(1 - \frac{a^3}{2r^3}\right)\cos\theta - \dot{a}\frac{a^2}{r}. \tag{1}$$

The velocity components of the relative velocity field $\boldsymbol{u} = \nabla\phi$ are obtained in the following form:

$$u_r = \dot{a}\frac{a^2}{r^2} - \left(1 - \frac{a^3}{r^3}\right)U\cos\theta, \tag{2a}$$

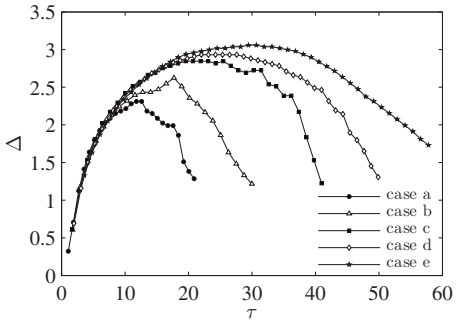

FIG. 7. Measurements of the dimensionless crater depth Δ as a function of dimensionless time τ.

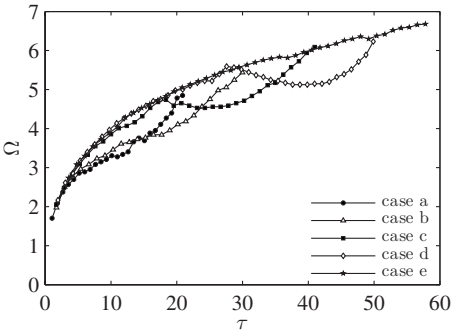

FIG. 8. Measurements of the dimensionless width depth Ω as a function of dimensionless time τ.

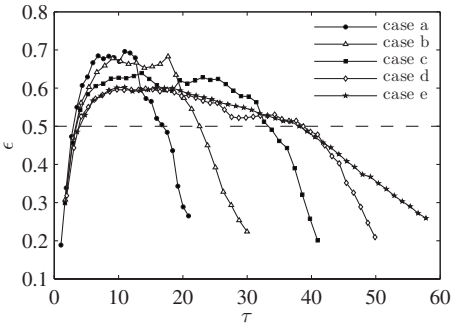

FIG. 9. Measurements of the crater shape factor $\epsilon = \Delta/\Omega$ as a function of dimensionless time τ.

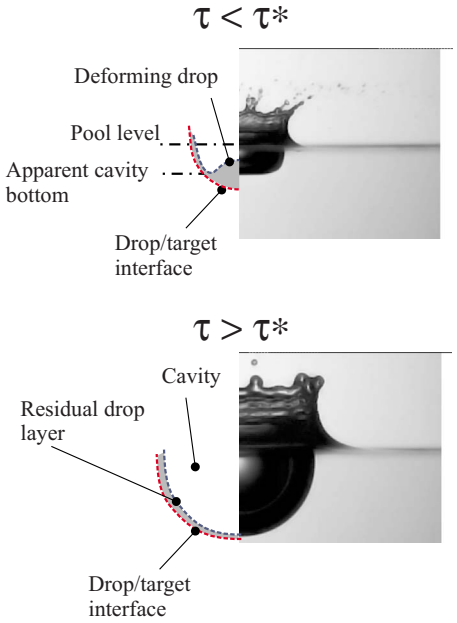

FIG. 10. (Color online) Phases of drop deformation and cavity formation.

$$u_\theta = \left(1 + \frac{a^3}{2r^3}\right) U \sin\theta. \tag{2b}$$

where $U \equiv \dot{z}_c$ is the velocity of the sphere translation. This velocity field satisfies the kinematic boundary conditions at the crater surface $r=a$ and far from the cavity at $r \to \infty$.

Pressure can now be determined using the nonstationary Bernoulli equation, which has to include an additional term accounting for the acceleration of the moving coordinate system,

$$\frac{\partial \phi}{\partial t} + \frac{1}{2}|\nabla \phi|^2 + \frac{p}{\rho} = f + g(z_c + r\cos\theta) - \ddot{z}_c r \cos\theta, \tag{3}$$

where $f(t)$ is a function of time determined from the boundary conditions. Since the pressure field far from the cavity, $r \to \infty$, is determined by the hydrostatic pressure, $p \to \rho g(z_c + r\cos\theta)$, Eq. (3) yields $f(t) = U^2/2$.

The pressure distribution $p_{\rm cr}(\theta, t)$ in the liquid at the crater surface, $r=a$, can now be obtained from the pressure field [Eq. (3)] with the help of Eq. (1),

$$\frac{p_{\rm cr}}{\rho} = \frac{U^2}{2}\left(1 - \frac{9}{4}\sin^2\theta\right) + g(z_c + a\cos\theta) + \frac{a\dot{U}}{2}\cos\theta + \frac{3\dot{a}^2}{2} + a\ddot{a} + \frac{3}{2}\dot{a}U\cos\theta. \tag{4}$$

It contains two unknown functions, $a(t)$ and $z_c(t)$, which have to be determined from the dynamic boundary conditions at the crater surface accounting for the capillary forces and gravity.

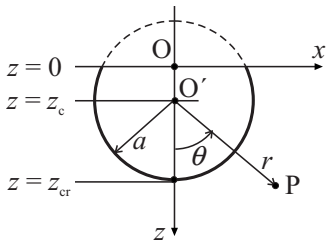

FIG. 11. Sketch of the cavity and definition of the fixed and moving reference frames.

B. Crater evolution at times $t > 2D/V$

1. Inviscid flow

At large times the pressure gradient in the thin drop spreading on the expanding crater is negligibly small. The Young-Laplace equation applied to the crater surface, $p_{\rm cr} + 2\sigma/a = 0$, cannot be satisfied exactly over the entire cavity surface. On the other hand expression (4) can be linearized near the cavity bottom, $\theta \approx 0$. The dynamic boundary condition can then be written in the form,

$$0 = -\frac{7U^2}{4} + gz_c + \frac{3\dot{a}^2}{2} + a\ddot{a} + \frac{2\sigma}{\rho a} + \left[\frac{9U^2}{4} + ga + \frac{a\dot{U}}{2} + \frac{3\dot{a}U}{2}\right]\cos\theta + O(U^2\theta^4). \tag{5}$$

It should be noted that at large times $U \ll \dot{a}$ since in all the considered cases the Froude number is small, therefore the last term in Eq. (5) is negligibly small in comparison with other terms.

Denote the dimensionless crater radius and axial coordinate of the center of the sphere as α and ζ. The dimensionless penetration depth is expressed as $\Delta = \zeta + \alpha$. Condition (5) yields a system of ordinary differential equations for $\alpha(\tau)$ and $\zeta(\tau)$ which can be written in dimensionless form,

$$\ddot{\alpha} = -\frac{3}{2}\frac{\dot{\alpha}^2}{\alpha} - \frac{2}{\alpha^2 \mathrm{We}} - \frac{1}{\mathrm{Fr}}\frac{\zeta}{\alpha} + \frac{7}{4}\frac{\dot{\zeta}^2}{\alpha}, \tag{6}$$

$$\ddot{\zeta} = -3\frac{\dot{\alpha}\dot{\zeta}}{\alpha} - \frac{9}{2}\frac{\dot{\zeta}^2}{\alpha} - \frac{2}{\mathrm{Fr}}. \tag{7}$$

The evolution of the crater can be now evaluated by numerical integration of the system of ordinary differential Eqs. (6) and (7), subject to the initial conditions which will be considered later.

It can be shown that in the limiting case $\mathrm{We} \to \infty$, $\mathrm{Fr} \to \infty$ the system [Eq. (6)] can be reduced to

$$\ddot{\alpha} = -\frac{3}{2}\frac{\dot{\alpha}^2}{\alpha}, \quad \ddot{\zeta} = -3\frac{\dot{\alpha}\dot{\zeta}}{\alpha} - \frac{9}{2}\frac{\dot{\zeta}^2}{\alpha}, \tag{8}$$

one partial solution of which is

$$\alpha = C_1(5\tau - C_2)^{2/5}, \tag{9}$$

where C_1 and C_2 are constants determined from the initial conditions. The relation $\alpha^{5/2} \sim t$ has been previously pro-

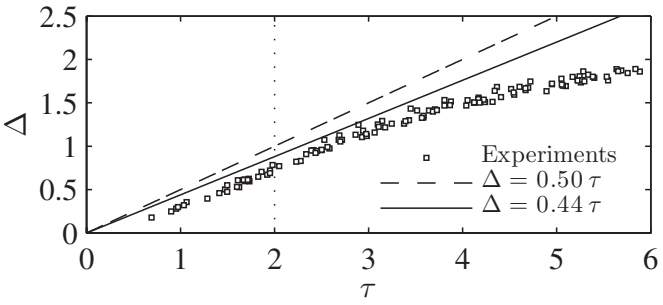

FIG. 12. Experimental and predicted dimensionless crater depth Δ at the initial stage for various impact parameters.

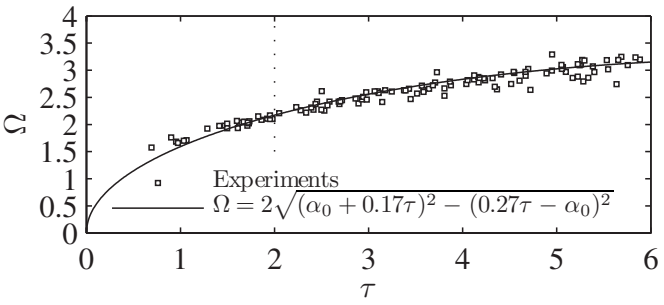

FIG. 13. Experimental and predicted dimensionless crater width Ω at the initial stage for various impact parameters. $\alpha_0=0.77$ has been found with a least mean square method.

posed in [12] from the considerations of energy balance. In [22] the constants in Eq. (9) has been estimated as $C_1=2^{-4/5}$ and $C_2=6$ and the corresponding solution is validated by comparison with the experimental data associated with very high impact velocities.

2. Evaluation of the effect of viscosity

At high Reynolds number flows the viscosity effects lead to the appearance of the viscous boundary layer near the crater free surface. This thin viscous flow ensures a shear stress at the free surface of the crater. On the other hand, since the layer is thin, the jump of the normal stresses through this layer is negligibly small. The Young-Laplace equation, which accounts for the viscous stresses, can be rewritten as

$$p_{\mathrm{cr}} - 2\mu\frac{\partial u_r}{\partial r} + \frac{2\sigma}{a} = 0 \quad \text{at} \quad r = a, \tag{10}$$

where the radial velocity of the outer flow u_r is defined in Eq. (1). The modified equation for the crater expansion is

$$\ddot{\alpha} = -\frac{3}{2}\frac{\dot{\alpha}^2}{\alpha} - \frac{2}{\alpha^2 \mathrm{We}} - \frac{1}{\mathrm{Fr}}\frac{\zeta}{\alpha} + \frac{7}{4}\frac{\dot{\zeta}^2}{\alpha} - \frac{4\dot{\alpha}}{\alpha^2\,\mathrm{Re}}, \tag{11}$$

$$\ddot{\zeta} = -3\frac{\dot{\alpha}\dot{\zeta}}{\alpha} - \frac{9}{2}\frac{\dot{\zeta}^2}{\alpha} - \frac{2}{\mathrm{Fr}} - \frac{12\dot{\zeta}}{\alpha^2\,\mathrm{Re}}. \tag{12}$$

It should be noted that results of computations of the crater depth using the systems [Eqs. (6), (7), (11), and (12)] in the considered range of impact parameters are practically undistinguishable, which indicates the fact that the effect of viscosity in the considered cases is negligibly small.

Since the order of the magnitude of $\dot{\alpha}$ is comparable with unity, the importance of the viscous terms in Eq. (11) in comparison with the capillary forces can be estimated by the capillary number $\mathrm{Ca}=\mathrm{Re}/\mathrm{We}$. The present analysis is therefore valid for the cases when the effect of viscous forces is small at $\mathrm{Ca} \gg 1$.

C. Initial stage of drop deformation, $t \lesssim 2D/V$: engineering approximation

In this study the well-known quasistationary model of initial drop penetration is modified to account for the flow associated with the cavity expansion. The boundary conditions [Eq. (10)] are not valid at this phase since they do not account for the pressure generated by the flow inside the deforming drop. At the initial stage the pressure distribution at the drop/outer liquid interface is roughly estimated neglecting the terms associated with gravity and cavity acceleration,

$$\frac{p_{\mathrm{init}}}{\rho} \approx \frac{U^2}{2}\left(1 - \frac{9}{4}\sin^2\theta\right) + \frac{3\dot{a}^2}{2} + \frac{3}{2}\dot{a}U\cos\theta. \tag{13}$$

Cavity expansion at this stage is determined by the pressure distribution in the deforming drop. The pressure in the deforming drop at the impact axis, $\theta=0$, can be roughly estimated from the Bernoulli equation for steady flows, whereas the pressure in the outer liquid can be evaluated using Eq. (13). The condition of the continuity of the pressure at the impact axis yields

$$\frac{p_{\mathrm{init}}(\theta=0)}{\rho} = \frac{U^2}{2} + \frac{3\dot{a}(\dot{a}+U)}{2} = \frac{(V-U-\dot{a})^2}{2}, \tag{14}$$

where $(U+\dot{a})$ is the velocity of propagation of the cavity tip, and $(V-U-\dot{a})$ is the velocity of drop deformation.

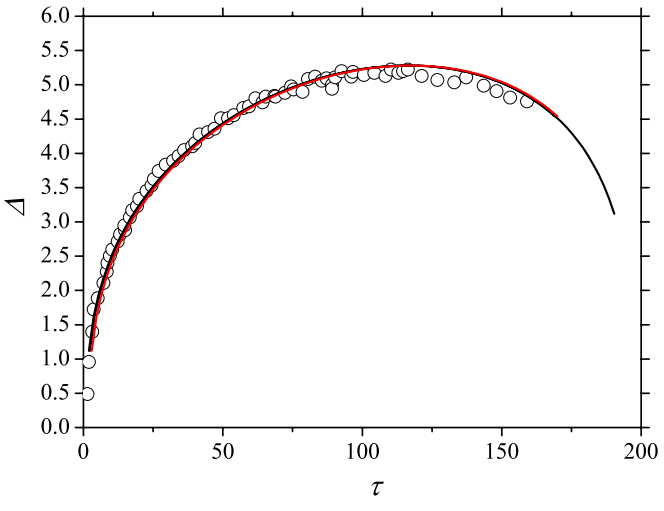

FIG. 14. (Color online) Penetration depth: comparison between the theoretical predictions and the experimental data from [18] (water, $D=4.5$ mm, $V=17.6$ m/s, $\mathrm{We}=19\,354$, $\mathrm{Fr}=6949$, $\mathrm{Re}=79\,541$). The Eqs. (6) and (7) are calculated using the initial conditions at $\tau^*=2$ and $\tau^*=3$. The theoretical results for these two values of τ^* are undistinguished from one another.

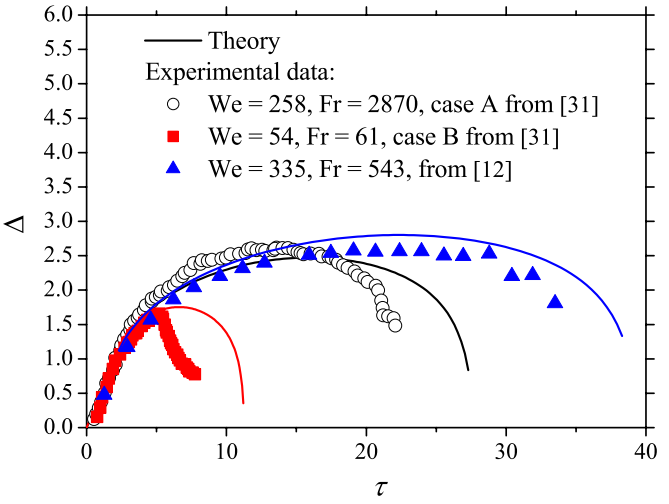

FIG. 15. (Color online) The dimensionless depth of crater penetration as a function of dimensionless time. Experimental data from [12,32] in comparison with the theoretical predictions.

The second equation is obtained from the condition of vanishing pressure p_{cr} at the free cavity surface ($z=0$). If the center of the sphere is located near to the liquid pool surface then this conditions yields

$$\frac{p_{cr}(\theta=\pi/2)}{\rho} = -\frac{5U^2}{8} + \frac{3\dot{a}^2}{2} = 0. \tag{15}$$

The roots of the system of Eqs. (14) and (15) are

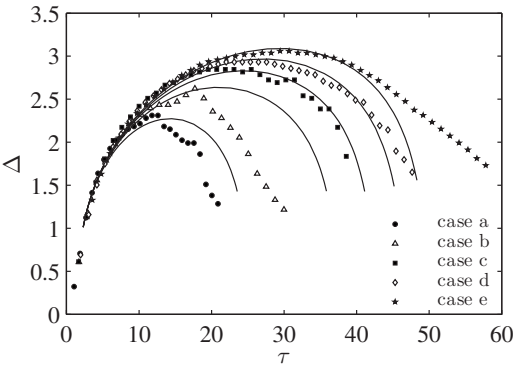

FIG. 16. The dimensionless depth of crater penetration as a function of dimensionless time. Comparison between experimental data (symbols) and theoretical predictions (curves) for various impact parameters listed in Table II.

$$U = \frac{-6-\sqrt{15}+3\sqrt{9+2\sqrt{15}}}{5+\sqrt{15}}V \approx 0.27V, \tag{16}$$

$$\dot{a} = \frac{1}{2}\sqrt{\frac{5}{3}}U \approx 0.17V. \tag{17}$$

The penetration velocity is therefore $U+\dot{a}\approx 0.44V$ which is very close to the experimental data, presented in Fig. 12 in dimensionless form and also very close to the earlier estimations $U+\dot{a}\approx 0.5V$ based on the constant velocity of an invis-

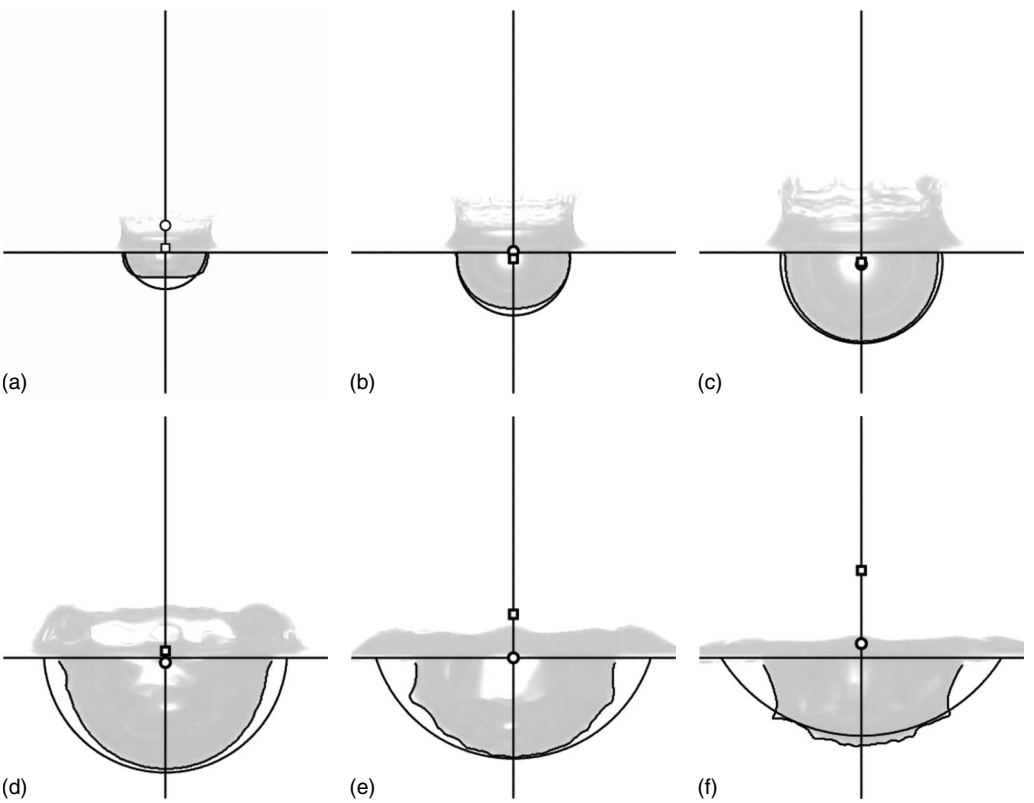

FIG. 17. Superposition of the theoretical model and the recorded images. The open circle symbol represents the center of the circle fitting the points A, B, C sketched in Fig. 6. The square symbol represents the center of the modeled crater.

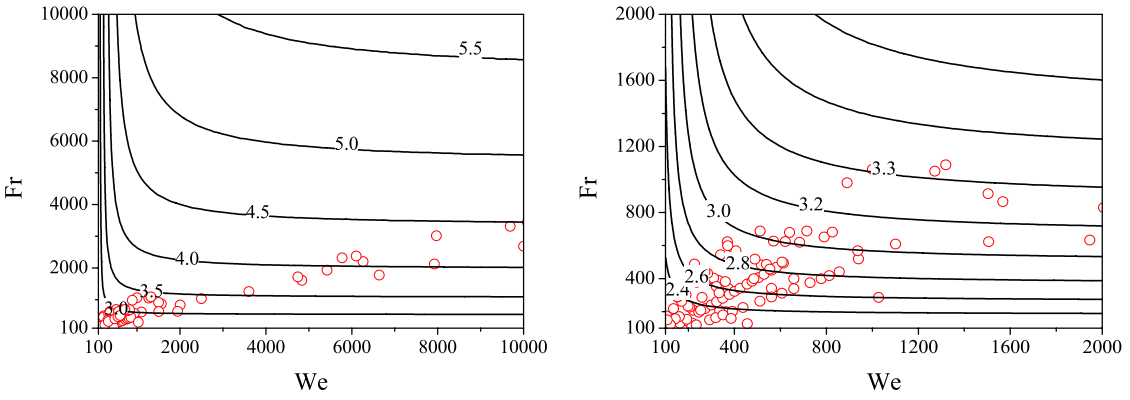

FIG. 18. (Color online) Contour plots of predicted dimensionless maximum crater depth for two different ranges of Weber and Froude numbers. Symbols correspond to the parameters used in the present study and in the experiments available in the literature.

cid jet of the same material as the target [26,27]. The straight continuous line $\Delta=0.44\tau$ shown in Fig. 12 only slightly overpredicts the experimental data. This overprediction can be explained by the fact illustrated in Fig. 10, that at $\tau<2$ we are not able to observe the drop/pool interface.

Noting that $\Delta=0$ at $\tau=0$ the values for $\alpha(\tau)$ and $\zeta(\tau)$ at the time period $\tau<2$ can be estimated in the following form:

$$\dot{\alpha}\approx 0.17, \quad \alpha\approx\alpha_0+0.17\tau, \quad \dot{\zeta}\approx 0.27, \quad \zeta\approx-\alpha_0+0.27\tau, \tag{18}$$

where α_0 is a constant associated with the initial cavity radius. It is obvious that these quantities do not depend on the impact parameters of the drop if the Reynolds, Weber, and Froude numbers are high. This fact has been clearly demonstrated in [23] for the analogous cases of drop impact onto a rigid dry substrate or onto a symmetry plane (the case associated with binary drop collisions).

The dimensionless width of the crater, Ω, can be estimated from the geometrical conditions,

$$\Omega=2\sqrt{\alpha^2-\zeta^2}\approx 2\sqrt{(\alpha_0+0.17\tau)^2-(0.27\tau-\alpha_0)^2}. \tag{19}$$

In Fig. 13 the experimental data for Ω are compared with the estimation [Eq. (19)], showing rather good agreement in the range $1<\tau<6$. The constant $\alpha_0=0.77$ is obtained by fitting.

Finally, taking $\tau^*=2$ the initial conditions for the calculations of the system [Eqs. (6) and (7)] are obtained from Eq. (18) as $\alpha(2)=1.11$, $\dot{\alpha}(2)=0.17$, $\zeta(2)=-0.23$, $\dot{\zeta}(2)=0.27$.

IV. RESULTS AND DISCUSSION

In Fig. 14, the theoretical predictions are compared with the experimental data from [18] with rather high values of We, Re, and Fr. In order to investigate the sensitivity of the theory to the initial conditions the predictions based on two typical times of drop deformations are shown: for $\tau^*=2$ and $\tau^*=3$. The results are apparently undistinguished. Similar agreement is obtained for the cases with smaller values of the impact parameters. In all the further calculations Eqs. (6) and (7) are integrated subject to the initial conditions corresponding to $\tau^*=2$.

Further comparisons between the model prediction and experiments for evolution of the penetration depth are shown in Fig. 15 (for existing experimental data from [12,32]) and Fig. 16. The agreement is good. As expected, the difference between experimental data and predicted values increases at the last part of the receding phase. Some discrepancy between the predictions and the experiments can be explained by the influence on the flow of the propagating capillary waves (not considered in the theory) and by the crater deformation at the bottom part, leading to the formation of the central jet. For instance cases *a* and *b* in Fig. 16 correspond to low impact velocity at which capillary waves significantly deform the crater shape.

Figure 17 shows a superposition of the crater predicted by the theoretical model onto the recorded images for the case *d* of Table II. The agreement between the theoretical predictions and the experimental shape of the cavity is particularly good at the bottom region of the crater ($\theta\ll 1$) where the model is valid. Some discrepancy appears when the shape of the crater is deformed by the capillary waves.

In Figs. 18 and 19, the predicted values for the maximum penetration depth and the corresponding time instant are represented as contour plots of Weber and Froude numbers. Additionally, in Fig. 18 a typical range of experimental parameters is marked by symbols. It can be clearly seen that in this

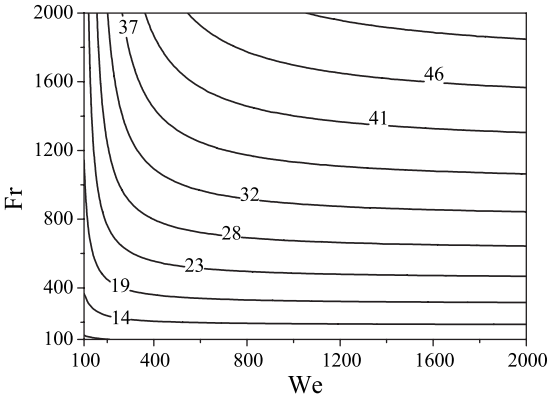

FIG. 19. Contour plots of predicted time instant corresponding to dimensionless maximum crater depth as a function of the Weber and Froude numbers.

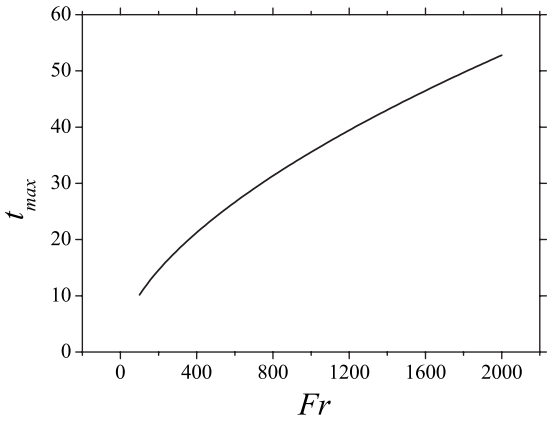

FIG. 20. Theoretically predicted dimensionless time $t_{\max}$ at We=2000 as a function of the Froude number.

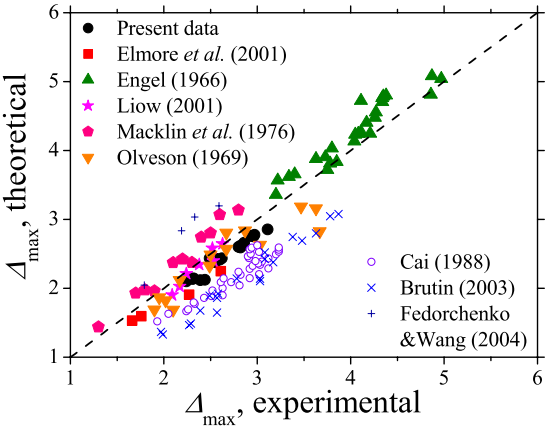

FIG. 21. (Color online) Maximum crater depth. Comparison of the theoretical predictions with the present experiments and with the experimental data from the literature.

field the maximum penetration diameter can be best represented almost exclusively by the Froude number while the effect of the Weber is minor. It explains why most of the existing empirical correlations are represented in the form $\Delta_{\max}(\mathrm{Fr})$. It is obvious that such correlations are not applicable for the cases associated with spray impact (with D usually is in the range from 5 to 500 μm), corresponding to much higher values of the Froude number.

A time scale for crater penetration can be roughly estimated for very high Weber numbers. Assume an asymptotic crater expansion $\alpha \approx t^{2/5}$ obtained in Eq. (9). Equation (7) for the sphere center can be reduced to the following form:

$$\ddot{\zeta} = -\frac{2}{\mathrm{Fr}} - \frac{6\dot{\zeta}}{5t} - \frac{9\dot{\zeta}^2}{4t^{2/5}}. \tag{20}$$

A solution of this equation is

$$\dot{\zeta} = -\frac{2\sqrt{2}t^{1/5}}{3\mathrm{Fr}^{1/2}}\frac{[CJ_{-11/8}(y) - J_{11/8}(y)]}{[CJ_{-3/8}(y) - J_{3/8}(y)]}, \quad y = \frac{15}{4\sqrt{2}}t^{4/5}\,\mathrm{Re}^{-1/2}. \tag{21}$$

where C is a constant, J is a Bessel function.

The effect of the motion of the sphere center becomes significant at the times t^* when $\dot{\zeta}$ is comparable with $\dot{\alpha} \sim t^{-3/5}$. It can be easily shown that this condition is satisfied at $t^* \sim \mathrm{Fr}^{5/8}$.

This time can be used as a scale for the value of $t_{\max}$ (corresponding to the maximum penetration depth) at very high Weber numbers. In Fig. 20 the dimensionless data for $t_{\max}$ is shown for We=2000. This data can be best fitted as $t_{\max} \sim \mathrm{Fr}^{0.56}$, which is in agreement with the estimations for t^*.

In Fig. 21, the results of the theoretical predictions of the dimensionless maximum crater depth are shown as a function of its experimental value for a wide range of Weber and Froude numbers. Also the existing experimental data from [8–14,16,32] are plotted in Fig. 21. A straight line corresponds to perfect agreement. The agreement of the theoretical predictions with our data is very good. It is not perfect for some data from different sources, but the tendency is predicted rather well. There is no systematic deviation of the predicted values from the experiments. It is interesting that the experimental data from the same sources lie on juxtaposed lines almost parallel to the theoretical curve. One possible explanation is the experimental errors, which is often not well documented. This fact is clearly illustrated in Figs. 1 and 2 and discussed in the "Introduction" section.

V. CONCLUSIONS

An experimental and analytical investigation of the crater formed by the impact of a drop on a deep liquid pool at sufficiently high Weber, Froude, and Reynolds numbers has been presented. Image processing has shown the shape of the crater to be very similar to a portion of a sphere in the region far from the unperturbed water level, where the edge becomes almost vertical. Potential flow theory has been used to model the flow around the crater. The equations of cavity expansion have been obtained from the balance of stresses at the crater interface. The model accounts for the effects of inertia, gravity, surface tension, and viscosity. The agreement between the theoretical predictions and the experimental data for the evolution of the penetration depth of the cavity is good. The proposed approach can be used for the description of submillimeter drop impacts, typical for spray/wall interaction, in which the effect of capillary forces is significant.

ACKNOWLEDGMENTS

A.B. acknowledges financial support of Cariplo, DAAD, and COST P21. G.E.C. acknowledges the partial funding from the National Project PRIN07. C.T. and I.V.R. would like to thank German Science Foundation (DFG) for financial support by the research Grant No. Tr 194/34 and the research grant in the framework of the Collaborative Research Center 568 (TP A1).

[1] A. M. Worthington, *A Study of Splashes* (Longmans, Green and Co., London, 1908).
[2] S. T. Thoroddsen, T. G. Etoh, and K. Takehara, Annu. Rev. Fluid Mech. **40**, 257 (2008).
[3] A. Prosperetti and H. N. Oğuz, Annu. Rev. Fluid Mech. **25**, 577 (1993).
[4] M. R. O. Panão and A. L. N. Moreira, Exp. Fluids **39**, 364 (2005).
[5] I. V. Roisman, K. Horvat, and C. Tropea, Phys. Fluids **18**, 102104 (2006).
[6] L. Schneider, N. Le Lostec, P. Villedieu, and A. Sadiki, Int. J. Multiphase Flow **36**, 261 (2010).
[7] M. Visaria and I. Mudawar, Int. J. Heat Mass Transfer **51**, 2398 (2008).
[8] D. Brutin, C. R. Mec. **331**, 61 (2003).
[9] Y. K. Cai, Acta Mech. Sin. **4**, 297 (1988).
[10] Y. K. Cai, Exp. Fluids **7**, 388 (1989).
[11] A. I. Fedorchenko and A.-B. Wang, Phys. Fluids **16**, 1349 (2004).
[12] J. L. Liow, J. Fluid Mech. **427**, 73 (2001).
[13] W. C. Macklin and G. J. Metaxas, J. Appl. Phys. **47**, 3963 (1976).
[14] K. L. R. Olevson, U.S. Geol. Surv. Prof. Pap. **650-D**, D189 (1969).
[15] V. Bertola (private communication).
[16] O. G. Engel, J. Appl. Phys. **37**, 1798 (1966).
[17] H. C. Pumphrey and P. A. Elmore, J. Fluid Mech. **220**, 539 (1990).
[18] O. G. Engel, J. Appl. Phys. **38**, 3935 (1967).
[19] H. N. Oğuz and A. Prosperetti, J. Fluid Mech. **219**, 143 (1990).
[20] K. A. Holsapple and R. M. Schmidt, J. Geophys. Res. **92**, 6350 (1987).
[21] L. A. Merzhievsky, Int. J. Impact Eng. **20**, 557 (1997).
[22] E. Berberović, N. P. van Hinsberg, S. Jakirlić, I. V. Roisman, and C. Tropea, Phys. Rev. E **79**, 036306 (2009).
[23] I. V. Roisman, E. Berberović, and C. Tropea, Phys. Fluids **21**, 052103 (2009).
[24] A. Dupré, Ann. Chim. Phys. **11**, 194 (1867).
[25] G. Taylor, Proc. R. Soc. London, Ser. A **253**, 296 (1959).
[26] G. Birkhoff, D. P. MacDougall, E. M. Pugh, and G. Taylor, J. Appl. Phys. **19**, 563 (1948).
[27] A. Y. Sagomonyan, *Penetration* (Moscow University Press, Moscow, 1974) (in Russian).
[28] A. Tate, J. Mech. Sci. **28**, 599 (1986).
[29] I. Frankel and D. Weihs, J. Fluid Mech. **216**, 213 (1990).
[30] A. L. Yarin, M. B. Rubin, and I. V. Roisman, Int. J. Impact Eng. **16**, 801 (1995).
[31] M. Rein, J. Fluid Mech. **306**, 145 (1996).
[32] P. A. Elmore, G. L. Chahine, and H. N. Oguz, Exp. Fluids **31**, 664 (2001).